

Quantum Andreev Oscillations in normal-superconducting-normal nanostructures

P. Rödiger,¹ P. Esquinazi,^{1,2,3,*} and N. García^{3,†}

¹*Division of Superconductivity and Magnetism, Institut für Experimentelle Physik II, Universität Leipzig, Linnéstraße 5, D-04103 Leipzig, Germany*

²*CMAM, Universidad Autónoma de Madrid, Cantoblanco, E-28049 Madrid, Spain*

³*Laboratorio de Física de Sistemas Pequeños y Nanotecnología, Consejo Superior de Investigaciones Científicas, E-28006 Madrid, Spain*

We show that the voltage drop of specially prepared normal-superconducting-normal nanostructures show quantum Andreev oscillations as a function of magnetic field or input current. These oscillations are due to the interference of the electron wave function between the normal parts of the structure that act as reflective interfaces, i.e. our devices behave as a Fabry-Perot interferometer for conduction electrons. The observed oscillations and field periods are well explained by theory.

PACS numbers: 85.35.Ds, 73.63.-h, 74.78.Na

The possibilities of exploiting quantum mechanical effects – with all the interferences and other phenomena occurring in real nano-devices – find new expectations that may lead to the fabrication of small devices with applications in new fields of technology as ballistic electronics and spintronics and flux devices combining normal and superconducting materials. Earlier work in semiconductors and STM experiments demonstrate the existence of quantum oscillations [1, 2]. Recently, spin-polarized resonant tunneling in magnetic tunneling junctions showed large changes in the magnetoresistance due to the interference of the carrier wave function [3]. In this work we seek after quantum mechanical interference effects in the magnetoresistance using normal-superconducting structures without tunneling. Because one of the characteristics needed is ballistic transport our experiments have to be done at low temperatures and the systems should be designed to have Fermi wavelength of the order or larger than their relevant size.

Assume a strip with a lateral structure M1/M2/M1, where M1 and M2 are two different materials with different Fermi energies E_F and lengths L_1 and L_2 and where the electrical current passes through them. Because of the different E_F 's between M1 and M2, the one particle potential can be described by a barrier U_2 of length L_2 in M2 that acts as a potential well where the wave function behaves coherently having multireflections, i.e. a kind of Fabry-Perot interferometer for electrons, a problem studied recently for the case of fluctuations in the magnetoresistance of graphene [4]. Inset in Fig. 1(a) shows the one-dimensional geometry of the system with the barrier $U_2(x)$ depending on the potential drop between the two ends of the trilayer. The transmittivity along such structure is [4, 5]

$$T(U, \alpha) = \frac{4\Delta E(\alpha)E(\alpha)}{4E(\alpha)\Delta E(\alpha) + U_2^2 \sin^2(2\pi L\sqrt{\Delta E(\alpha)\frac{2m}{\hbar^2}})}. \quad (1)$$

The parameters in (1) are: $\Delta E(\alpha) = E(\alpha) - U_2$; $E(\alpha) = (E_F + U) \cos^2(\alpha)$ is the energy of the incoming particles

forming an angle α to the interface, m the electronic mass and $\hbar = h/2\pi$. Applying a potential to the trilayer the potential in M2 is $U_2(x) = U_0 - (U/L_2)(x - L_1)$ ($L_1 \leq x \leq L_1 + L_2$). The solution to this problem can be obtained as combination of Airy functions [1, 2]. A good approximation is to take the trapezoidal rule, i.e. $U_2(x) \approx U_0 - 0.5U$ and calculate $T(U)$ following (1) as shown in Fig. 1(a). Interference effects require ballistic transport in the potential region M2 with conveniently flat interfaces to avoid multiple reflections. We will use M2 as a superconductor (S) or as normal metal (N) and vice versa for M1, of appropriate lengths.

When M2 is a superconductor the current will be controlled by Cooper pairs Andreev currents if $U < \Delta$ (Δ is the superconducting gap) [6]. However at higher U the current is controlled by quasiparticles and for $U > 3\Delta$ we have practically conduction between normal materials [6, 7, 8]. The solution for the current I is in this case:

$$I(U) = A \int_0^U \left[1 - \frac{|(1-a^2)|^2(1-|T|)}{|1-a^2(1-|T|)|^2} + \frac{a^2|T|^2}{|1-a^2(1-|T|)|^2} \right] dU', \quad (2)$$

where the term inside the integral is the Andreev conductance (in units of quantum of conductance) $g_{NS}(U, T)$ [7, 8], which depends on T in the *normal state*; $a = (U/\Delta) - [(U/\Delta)^2 - 1]^{0.5}$; A is a constant that depends on the junction geometry and on the integration average on α . The solution for I is depicted in Fig. 1(b). Note that: (a) g_{NS} oscillates as a function of the energy drop U because of the resonances in $T(U)$ and it tends to $T(U)$ when the product $U/\Delta \gg 1$, see Fig. 1(a). (b) The measured voltage drop will oscillate as a function of I and, at constant I , as a function of the magnetic field B through $U(B)/e \propto V(B) = IR(B)$, where $R(B)$ is the, in general, non-oscillatory magnetoresistance of the sample.

The increment of the applied voltage drop ΔV needed to obtain one oscillation is given by $\Delta V \sim \pi^2(\hbar^2/m)(1/L_2^2)$. It can be seen that for m of order of

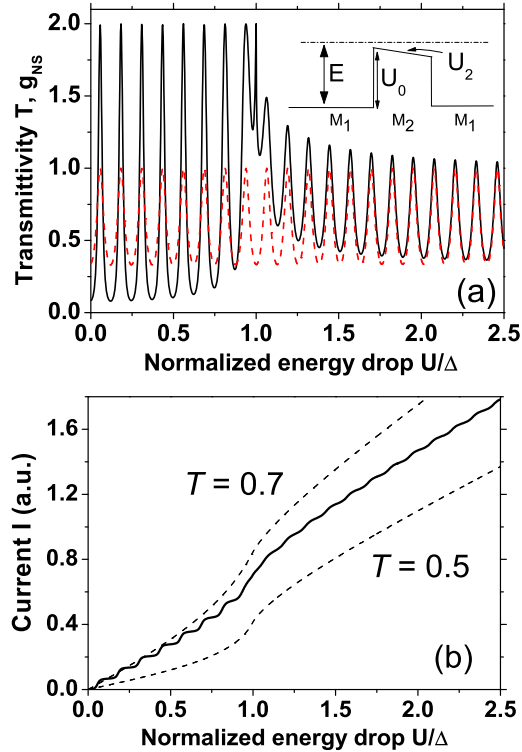


FIG. 1: (a) Inset shows the energy diagram for a M1/M2/M1 structure with a barrier $U_2(x)$ such that $U_2(L_1) = U_0$ (the energy drop at M1 has been neglected for clarity). Main panel shows the transmittivity T from (1) for M2 in the normal state (dashed line) as well as the Andreev conductance g_{NS} (continuous line) vs. normalized energy drop U/Δ at M2. (b) Carrier current I vs. normalized energy drop after (2). The two dotted lines are calculated for constant transmittivity $T = 0.5, 0.7$ for a NS bilayer that shows no oscillations. The middle curve that shows the oscillatory behavior is obtained with T from (1), see panel (a). Note that the strength of the oscillations is larger for $U < \Delta$.

the free mass the needed voltage change is $\Delta V \sim \mu\text{V}$ to mV for L_2 in the micro and nanometer range, respectively. For example, if the superconducting gap is less than 1 meV with $L_2 \sim 10$ nm we need to have voltage drops of several millivolts, i.e. the situation is practically a trilayer with normal conducting materials. However, for $L_2 \sim 1 \mu\text{m}$, $\Delta V \sim 1 \mu\text{V}$.

The NSN and SNS structures were produced combining electron beam lithography with the deposition features of a FEI NanoLab XT 200 microscope. The tungsten precursor in the gas injection system enables us to fabricate homogeneous, amorphous superconducting tungsten-carbide (WC) micro- and nano-structures by Ga^+ -ion beam induced deposition (IBID) with critical temperature $T_c = 4 - 5$ K [9]. The deposition param-

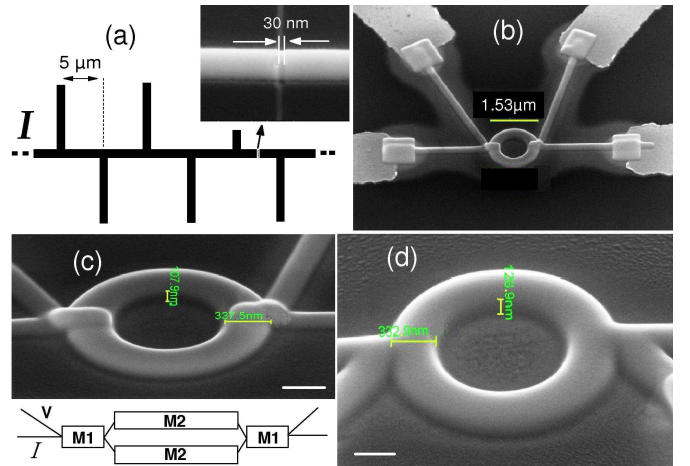


FIG. 2: (a) Sketch of the superconducting long strip with voltage electrodes normal to it. The distance between them was $5 \mu\text{m}$. The width and thickness were 200 nm and 80 nm . The SEM picture at the upper right shows the region at and around one of the slits. (b) SEM picture of the WC ring labeled WR_2 with the contacts pads deposited after the ring. (c) A blow out of the same ring as in (b). The cartoon below shows the equivalent circuit of the ring with M1 and M2 the normal and superconducting paths. (d) SEM picture of ring WR_0 produced in a single-step procedure. The white bars in (c) and (d) indicate 300 nm distance.

eters were 30 kV accelerating voltage, 10 pA Ga^+ -ion current and 50% overlap. All samples were produced on $5 \times 5 \times 0.53 \text{ mm}^3$ silicon substrates with 150 nm insulating SiN layer. The lithographically prepared multi-electrode structure was connected to a multi-electrode chip and this was fixed in a magneto-cryostat system. The resistance measurements were done using four-wires method with AC Linear Research LR700 bridge with a multiplexer. DC Current-voltage ($I - V$) characteristics as well as field B dependent $V(B, I)$ curves were obtained using a Keithley 2182 nanovoltmeter with a 6221 current source.

We will discuss first the results for SNS-type nanostructures. A $\sim 60 \mu\text{m}$ -long WC strip with eight voltage electrodes at a distance of $5 \mu\text{m}$ was fabricated in a single-step IBID procedure enabling us to measure simultaneously different portions of the strip (channels 1 to 8, see Fig. 2(a)). To produce narrow, normal-conducting paths (M2) within the superconducting strip with high-quality SN interfaces, minimizing preparation time and costs, we irradiated it locally at the middle of different voltage channels with the same Ga^+ -ion beam (30 kV , 1 pA , zero nominal thickness). In general, ion irradiation strongly degrades the superconducting properties of a material, see e.g. Ref. 10. The length of the slits was $L_2 \simeq 30 \text{ nm}$, see Fig. 2(a). As reference some channels were left without slits. The sample W-SD-1 discussed here showed a $T_c \simeq 4.3 \text{ K}$ defined at half-resistance at

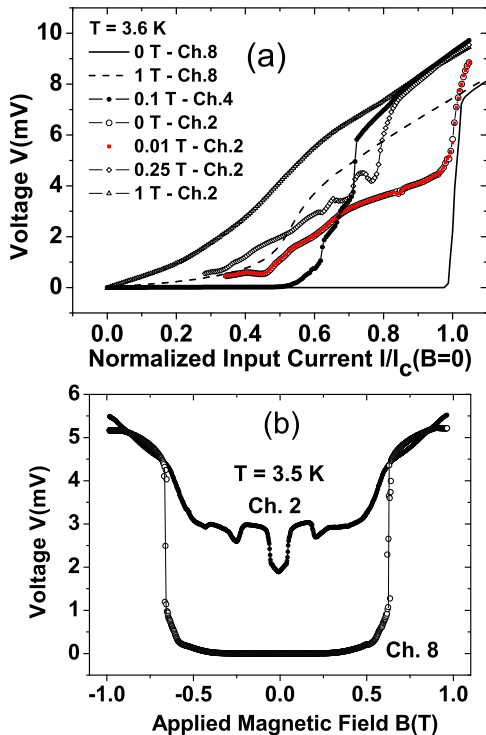


FIG. 3: (a) Voltage (V) vs. input current (I) normalized by the critical current $I_c(0) = 19.1 \mu\text{A}$ at zero field at 3.6 K, measured for two different channels, each one with one slit: Ch. 2 at $0 \text{ T} \leq B \leq 1 \text{ T}$ and Ch. 4 at 0.1 T applied field. Two curves were obtained for Ch. 8 (without irradiation, $I_c(0) = 16 \mu\text{A}$) at 0 T and 8 T of the same strip sample. (b) Voltage vs. applied field for Chs. 2 and 8 at 3.5 K and for an input current of $12 \mu\text{A}$.

$B = 0 \text{ T}$. At input currents $I \lesssim 1 \mu\text{A}$ and $B = 0 \text{ T}$ the slits short circuit the strip at $T < 4 \text{ K}$ due to the large proximity effect as observed, for example, in Al thin films [11]. At higher currents or fields the slits show normal conducting behavior.

Figure 3(a) shows the voltage vs. current measured for Chs. 2, 4 and 8 at 3.6 K at different magnetic fields applied normal to the input current. At zero field and at $I < 16 \mu\text{A}$ the voltage drop in the homogeneous, unirradiated Ch. 8 is below the 1 nV resolution. At the critical current $I_c \simeq 16 \mu\text{A}$ the voltage jumps to a value close to that expected for that conducting path in the normal state, which has a resistance of $\simeq 500 \Omega$. Within experimental resolution this curve does remain without changes for an applied field of 0.01 T. At $B > 0.01 \text{ T}$ the critical current decreases and flux-flow behavior is observed. As example, Fig. 3(a) shows the data obtained at $B = 1 \text{ T}$. No hysteretic behavior was observed, which rules out heating effects. Channels 2 and 4 show the

voltage across two different SNS structures, each with a single slit. At $B = 0 \text{ T}$ and 0.01 T the voltage drop below $I_c(0)$ is several orders of magnitude larger than that obtained for Ch. 8 (as example we show the signal of Ch. 2 in Fig. 3(a)). At fields below 1 T and at $T = 3.6 \text{ K}$ Chs. 2 and 4 show clear oscillatory behavior similar to that shown in Fig. 1(b), in contrast to that of Ch. 8. At higher fields ($B \gtrsim 1 \text{ T}$) the flux-flow contribution prevails and the curves for all channels resemble qualitatively (Chs. 2 and 8 response is shown in Fig. 3(a)). The quantum mechanical resonances can be also observed in $V(B)$ at constant current, see Fig. 3(b), because the magnetic field changes the voltage drop at the normal conducting path due to its intrinsic magnetoresistance changing therefore $T(U)$. The oscillation amplitude is of the order of mV, i.e. larger than the superconducting gap $\Delta < 0.4 \text{ meV}$, in agreement with the model if $L_2 \simeq 30 \text{ nm}$. Note that the free electron gas model used here provides the general physics of the phenomenon. More detailed analysis of the band structure of M1 and M2 can explain the delicate structure of the experimental curves.

In what follows we discuss NSN-type nanostructures with long superconducting M2 paths. For reasons that will become clear below and as an example of the deposition possibilities we prepared NSN ring structures, see Fig. 2(b-d). To do the normal M1 paths we used a two-step IBID procedure, which consists in re-deposit WC material on the top of the already deposited superconducting ring path as the electrical contacts of the rings WR_1 and WR_2 . In this case the material M1, between the superconducting electrodes and ring, shows a lower T_c as the resistance transition indicates, see Fig. 4(a). The T - and B -dependent measurements reveal that we have normal (semi)conducting interfaces between the electrodes and the ring structure at $T \gtrsim 4.7 \text{ K}$ at $B = 0 \text{ T}$. To check that the observed two-step transition as well as the oscillations described below are not related to the ring structure itself, a one-piece (e.g. one-step procedure) ring WR_0 was prepared in which the contacts and ring are produced in a single-step IBID using especial bitmap pattern generator features, see Fig. 2(d).

Because in our NSN ring structures $L_2 \sim 3 \mu\text{m}$, we expect oscillations in the submicrovolt range. In agreement with the model these oscillations are nicely observed between $\sim 4.9 \text{ K}$ and 4.7 K and around 0.2 T, see Fig. 4(b). The field was always applied normal to the ring area. No oscillations were observed at lower temperatures, below the critical line of the M1 material, above the critical line of the ring as well as for the homogeneous ring WR_0 in the whole T, B -range. Note that the model [4] applies only at $T = 0 \text{ K}$. However, the equivalent maximum energy of the oscillations in the ring structure is $\sim 50 \text{ neV}$ much smaller than the thermal energy of 0.4 meV . This indicates that the conducting path M1 is a narrow band semiconductor because only in this case the temperature excitation of electrons, intraband or to other conduction

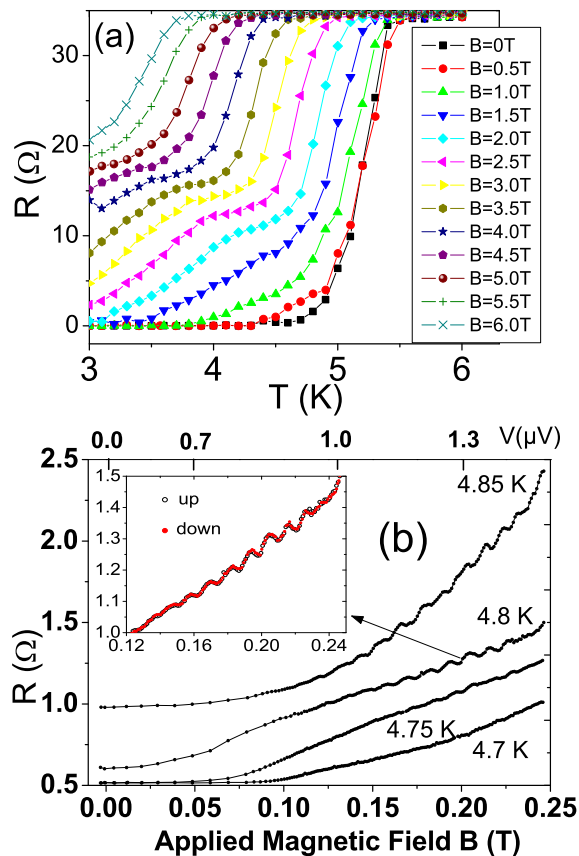


FIG. 4: (a) Resistance vs. temperature at different applied fields of ring WR_1 measured with a current of $1 \mu A$, which is 30 times smaller than I_c at similar B, T . The critical field of the superconducting transition of the ring itself (upper transition) follows $B_{c2}(T) \simeq 8.1[T](1 - (T/T_c)^2)$ with $T_c \simeq 5.2$ K. (b) Resistance of the ring WR_1 vs. field at different T . The inset blows out part of the 4.8 K curve measured increasing and decreasing field. The dimensions of the ring WR_1 were $(2.57, 1.6, 0.15) \mu m$ for the outer- and inner-diameter and thickness, respectively.

band, is small.

We expect that the field period of the oscillations should be very sensitive to the properties of the normal M1 part of the NSN structure and therefore it should change from sample to sample. This is indeed the case. The ring sample WR_2 shows a field frequency of 0.1 T, about ten times larger than for sample WR_1 , implying that the M1 material should have a larger E_F according to the model.

The highly reversible behavior of the oscillations at all temperatures and fields (an example at 4.8 K is shown in the inset of Fig. 4(b)) does not support an interpretation of the oscillations based on Josephson-like junc-

tion at the contact positions. Magnetoresistance oscillations were observed in superconducting mesoscopic rings at very low fields and explained by the oscillatory behavior of the critical current density $I_c(B)$ at $T \sim T_c(B)$ [12]. Oscillations in the conductance were also observed in normal metal rings with two tunnel junctions due to the magneto-electric Aharonov-Bohm effect [13]. In those works the field period is related to the field needed to add one (or two) flux quantum in the ring area, which for the geometry of our rings would give ~ 0.5 mT - 2.5 mT, far below the experimental observed value of 12 mT - 100 mT for the rings WR_1 and WR_2 , respectively.

In summary, in this work we showed the existence of quantum Andreev oscillations in the magnetoresistance of NSN and SNS nanostructures. These oscillations are observed also as a function of magnetic field due to the intrinsic, non-oscillatory magnetoresistance effect of the structure. The oscillations and their field period are well explained by theory taking into account ballistic transport and carrier wave function interference within the structure. The effects here reported might be used to study granular, superconducting materials, when neither Meissner effect nor percolation can be observed. Similar oscillations as in our NSN structures were recently observed in thin mesoscopic structures of graphite [14]. This kind of quantum mechanical resonances in the voltage should appear in every nanostructure composed by different materials, if the electronic conduction is ballistic and the roughness of the interfaces is small enough.

We gratefully acknowledge the collaboration and support of K. Schindler, J. Barzola-Quiquia, and M. Ziese. This work was done with the support of a HBFEG-grant no. 036-371, the Spanish CACyT and Ministerio de Educación y Ciencia.

* Electronic address: esquin@physik.uni-leipzig.de

† Electronic address: nicolas.garcia@fsp.csic.es

- [1] G. Binnig, K. H. Frank, H. Fuchs, N. García, B. Reihl, H. Rohrer, F. Salvan, and A. R. Williams, *Phys. Rev. Lett.* **55**, 991 (1985).
- [2] K. H. Gundlach, *Solid State Electron.* **9**, 949 (1966).
- [3] S. Yuasa, T. Nagahama, and Y. Suzuki, *Science* **297**, 234 (2002), C. W. Miller et al., *Phys. Rev. Lett.* **99**, 047206 (2007), T. Niizeki, N. Tezuka and K. Inomata, *Phys. Rev. Lett.* **100**, 047207 (2008).
- [4] N. García, arXiv:0706.0135.
- [5] A. Messiah, *Quantum Mechanics* (Dover Books on Physics, 1999), ISBN 0-486-40924-4.
- [6] A. F. Andreev, *Sov. Phys. JETP* **19**, 1228 (1964).
- [7] G. E. Blonder, M. Tinkham, and T. M. Klapwijk, *Phys. Rev. B* **25**, 451 (1982).
- [8] N. García, F. Flores, and F. Guinea, *J. Vac. Sci. Technol. A* **6**, 323 (1988).
- [9] D. Spoddig, K. Schindler, P. Rödiger, J. Barzola-Quiquia, K. Fritsch, H. Mulders, and P. Esquinazi, *Nanotechnology* **18**, 495202 (2007).

- [10] S. I. Woods, A. S. Katz, M. C. de Andrade, J. Herrmann, M. B. Maple, and R. C. Dynes, *Phys. Rev. B* **58**, 8800 (1988).
- [11] Y. Kwong, K. Lin, M. Park, M. Isaacson, and J. Parpia, *Phys. Rev. B* **45**, 9850 (1992).
- [12] V. V. Moshchalkov, L. Gielen, M. Dhallé, C. V. Haendonck, and Y. Bruynseraede, *Nature* **361**, 617 (1993).
- [13] A. van Oudenaarden, M. H. Devoret, Y. V. Nazarov, and J. E. Mooij, *Nature* **391**, 768 (1998).
- [14] P. Esquinazi, N. García, J. Barzola-Quiquia, M. Muñoz, P. Rödiger, K. Schindler, J.-L. Yao, and M. Ziese, arXiv:0711.3542.